

DIFFUSE γ -RAY EMISSION FROM MISALIGNED ACTIVE GALACTIC NUCLEI

M. DI MAURO

Physics Department, Torino University, and Istituto Nazionale di Fisica Nucleare, Sezione di Torino, via Giuria 1, 10125 Torino, Italy

F. CALORE

II. Institute for Theoretical Physics, University of Hamburg, Luruper Chaussee 149, 22761 Hamburg, Germany

F. DONATO¹

Physics Department, Torino University, and Istituto Nazionale di Fisica Nucleare, Sezione di Torino, via Giuria 1, 10125 Torino, Italy

M. AJELLO

Space Sciences Laboratory, University of California, Berkeley, CA, 94720

L. LATRONICO

Istituto Nazionale di Fisica Nucleare, Sezione di Torino, via Giuria 1, 10125 Torino, Italy

Submitted to The Astrophysical Journal.

ABSTRACT

Active galactic nuclei (AGN) with jets seen at small viewing angles are the most luminous and abundant objects in the γ -ray sky. AGN with jets misaligned along the line-of-sight appear fainter in the sky, but are more numerous than the brighter blazars. We calculate the diffuse γ -ray emission due to the population of misaligned AGN (MAGN) unresolved by the Large Area Telescope (LAT) on the *Fermi* Gamma-ray Space Telescope (*Fermi*). A correlation between the γ -ray luminosity and the radio-core luminosity is established and demonstrated to be physical by statistical tests, as well as compatible with upper limits based on *Fermi*-LAT data for a large sample of radio-loud MAGN. We constrain the derived γ -ray luminosity function by means of the source count distribution of the radio galaxies (RGs) detected by the *Fermi*-LAT. We finally calculate the diffuse γ -ray flux due to the whole MAGN population. Our results demonstrate that the MAGN can contribute from 10% up to nearly the entire measured Isotropic Gamma-Ray Background (IGRB). We evaluate a theoretical uncertainty on the flux of almost an order of magnitude.

1. INTRODUCTION

The *Fermi*-LAT has measured the Isotropic Gamma-Ray Background (IGRB) with very good accuracy from 200 MeV to 100 GeV (Abdo et al. 2010c). Increased statistics from additional LAT data are expected to allow the IGRB to be measured over an even broader energy range. The nature of the IGRB is still an open problem in astrophysics. Blazars and star-forming galaxies contribute 20%-30% of the IGRB (Ackermann et al. 2012a; Abdo et al. 2010d), and with a compatible spectral slope. Blazars are Active Galactic Nuclei (AGN) whose jets are oriented along the lines-of-sight (l.o.s.). Their luminosity is quite high, due to Doppler boosting effects. For the same reasons, AGN with axes misaligned with respect to the line-of-sight (hereafter MAGN) have weaker luminosities but are expected to be more numerous by a factor $2\Gamma_L^2$ (where Γ_L is the Lorentz factor) (Urry & Padovani 1995). About 10% of the observed AGN are radio-loud. According to the unified model, AGN are classified as a function of their jet orientation with respect to the l.o.s. (Urry & Padovani 1995). A jet misalignment of about 14° indicates the separation between blazars and non-blazar, *i.e.* misaligned, objects. In the unified model, radio galaxies (RGs) are those objects which, on average, have their jets pointing at $> 44^\circ$ from our l.o.s., while MAGN below this

angle and above about 14° are generally identified with radio quasars (Barthel 1989). RGs are classified in turn into two categories based upon their radio morphology (Fanaroff & Riley 1974). The first class of objects, named Fanaroff-Riley Type I (FRI), is preferentially found in rich clusters and hosted by weak-lined galaxies, and has a low luminosity radio emission (which peaks near the center of the AGN and shows two-sided jets dominated emission). Fanaroff-Riley Type II (FRII) galaxies present a high luminosity radio emission dominated by the lobes, while jets and core, when detected, are faint. The hot spots, generally not present in FRIs, are usually detected at the ends of the lobes. The threshold in luminosity for discriminating between FRI and FRII is about $10^{25} \text{ W Hz}^{-1} \text{ sr}^{-1}$ at 178 MHz (Fanaroff & Riley 1974). FRIs and FRIIs are considered the parent populations of BL Lacertae objects (BL Lacs) and flat spectrum radio quasars (FSRQs), respectively.

Given the large numbers of known radio-loud MAGN, and in some analogy with blazars, it is expected that a non-negligible contribution to the IGRB might be attributable to the MAGN population. The aim of this paper is the estimation of the γ -ray diffuse emission produced by the cosmological population of MAGN. We investigate the absolute level of the MAGN γ -ray flux and quantify the possible uncertainties of our prediction.

The paper is organized as follows: in Sect. 2 we derive the correlation between radio core ($L_{r,\text{core}}$) and γ -ray luminosi-

¹ corresponding author: donato@to.infn.it

ties (L_γ) from a sample of 12 MAGN detected by *Fermi*-LAT. The robustness of the $L_\gamma - L_{r,\text{core}}$ correlation is tested in Sect. 3 by computing the 95% confidence level (C.L.) upper limits on the γ -ray flux of a sample of radio-loud MAGN with 4-years of *Fermi* data. In Sect. 4 two statistical tests are performed on the core radio and γ -ray data in order to exclude spurious effects in the correlation between luminosities. By assuming the relation found between L_γ and $L_{r,\text{core}}$, in Sect. 5 we model the γ -ray luminosity function (GLF) from the radio luminosity function (RLF). We discuss the consistency of the models in Sect. 6, where we compare our predictions of the source count distribution and compare them to the *Fermi*-LAT data. Our findings for the contribution of an unresolved population of MAGN to the IGRB are presented in Sect. 7, together with the evaluation of the relevant uncertainties. Finally, we draw our conclusions in Sect. 8.

Throughout the paper we adopt a standard Λ CDM cosmology with parameters: $H_0 = 70 \text{ km s}^{-1} \text{ Mpc}^{-1}$, $\Omega_M = 0.27$, $\Omega_\Lambda = 0.73$.

2. THE CORRELATION BETWEEN γ -RAY AND RADIO LUMINOSITY

The calculation of the diffuse emission from unresolved (*i.e.* not detected by the *Fermi*-LAT) MAGN relies on the γ -ray luminosity function for that specific population. The physical processes underlying the emission of γ rays in RGs are not firmly established. It is believed that the bulk of the radiation is generated via synchrotron self-Compton (SSC) scatterings, where the seed photons are provided by synchrotron emission by the same electron population (Maraschi et al. 1992). It is not excluded that an external inverse Compton (EC) scattering occurs off photons external to the jet (Dermer & Schlickeiser 1993). Typically the EC scenario requires that the inverse-Compton (IC) γ radiation originates relatively close to the center of the AGN, within the central parsec, while the SSC γ rays come from the jet outside that region. A relevant contribution to a detectable γ -ray emission from the external lobes is thought to be unlikely. The lobe contribution was evaluated in Stawarz et al. (2006); Massaro & Ajello (2011). Ultra-relativistic electrons in the lobes emit synchrotron radiation in the radio band and are able to up-scatter low energy photons via IC scattering to high energies, provided a high enough electron density is available. The dominant contribution is expected to be from CMB photons. The IC/CMB scattered emission in the lobes of distant galaxies is generally well observed in the X-ray band. Extended γ -ray emission from regions corresponding to radio lobes has been detected from Centaurus A (Abdo et al. 2010a). Such emission, if interpreted in terms of IC scattering of electrons with ambient photons, requires high-energy electrons in the lobes, but it is unclear how common this is in other RGs. In what follows, we assume the γ -ray radiation originates in the central region of the source, as is predicted from both SSC and EC scenarios.

The FRI and FRII galaxies show a strong emission in a wide radio band, spanning from hundreds of MHz up to tens of GHz. These photons are ascribed to the synchrotron emission of highly relativistic electrons moving in the entire region of the source. The total radio flux has been measured for hundreds of FRI and FRII galaxies. For a number of these galaxies the emission from the central unresolved region of an arcsecond scale, often referred to as the core, is detected as well. In the first and the second catalogs of LAT AGN sources (Abdo et al. 2010b; Ackermann et al. 2011b) *Fermi*-LAT has

reported the detection of 15 MAGN, which can be classified into 10 FRI and 5 FRII galaxies (although with some caveats, see below). Abdo et al. (2010b) report on the observation of 3C 78, PKS 0625-35, 3C 207, 3C 274, Centaurus A, NGC 6251, 3C 380, 3C 120, 3C 111, 3C 84, PKS 0943-76, while Centaurus B, Fornax A and IC 310 have been reported in the second LAT catalog (2FGL) (Nolan et al. 2012a,b) (for Centaurus B see also Katsuta et al. (2013)) and a Pictor A identification has been discussed in Brown & Adams (2012).

In the absence of predictions for the γ -ray luminosity function, we follow a phenomenological approach to relate the γ -ray luminosity to the radio luminosity. The latter is phenomenologically much better established, given the high number of detected MAGN in the radio frequencies. A possible correlation between radio and γ -ray luminosities has been proposed for blazars using the Energetic Gamma Ray Experiment Telescope (EGRET) data (Padovani et al. 1993; Stecker et al. 1993; Salamon & Stecker 1994; Dondi & Ghisellini 1995; Narumoto & Totani 2006). Recently, the connection between radio and γ -ray fluxes has been explored for both the FSRQs and BL Lacs detected by *Fermi*-LAT during its first year of operation (Ackermann et al. 2011a; Ghirlanda et al. 2011). On a similar basis, the relation between radio emission and γ -ray data has been studied for three FRI galaxies observed by EGRET (Ghisellini et al. 2005), as well as for FRI and FRII galaxies with 15 months of data taken with *Fermi*-LAT (Inoue 2011; Abdo et al. 2010b). Variability studies for FRI galaxies support the hypothesis of the compactness of the γ -ray source (Abdo et al. 2010b; Grandi et al. 2012a), even if a non-negligible γ -ray counterpart in radio lobes has been observed in Centaurus A (Abdo et al. 2010a). The situation for the FRII population is less definite. A recent *Fermi*-LAT analysis of the FRII 3C 111 galaxy (Grandi et al. 2012b), together with a multi-frequency campaign conducted in the same period, localizes the GeV photons from 3C 111 in a compact, central region associated with the radio core.

The main radio and γ parameters of all the MAGN observed by *Fermi*-LAT are reported in Table 1. The radio data have been chosen to be the closest in time to *Fermi*-LAT data taking. Whenever a significant variability has been found, we have selected radio data almost contemporary to the γ -ray observations. Radio data have been taken with the Very Large Array (VLA) for all the objects except NGC 6251, measured with the Very Long Baseline Interferometer (VLBI). The linear size scales explored by the instruments depend on the redshift of the sources. In our sample, it varies from about 0.01 kpc to a few kpc, except for NGC 6251 (0.002 kpc) and 3C 380. Data for 3C 380 are taken from Effelsberg observations with a high resolution. However, this source shows a compact steep spectrum radio morphology and the radio flux from the central region is close to the total emission and to the flux measured with a few arc sec scale¹. For 3C 84 the variability is very pronounced and we have therefore excluded it from our correlation analysis. IC 310 lacks measurements of the core at 5 GHz, and the total radio flux is very faint. For PKS 0943-76 only upper limits for the core are given. For these reasons, these two galaxies are listed but not considered in our analysis. The photon index Γ valid between 0.1 and 10 GeV, and the *Fermi*-LAT flux integrated for $E_\gamma > 0.1$ GeV have been taken from Abdo et al. (2010b) for 3C 78, 3C 111, 3C 120 and from Nolan et al. (2012b) for the remaining objects.

¹ <http://3crr.extragalactic.info/cgi/database>

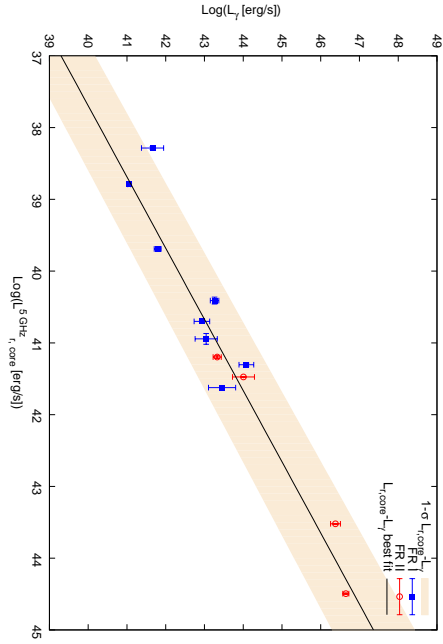


Figure 1. Observed γ -ray luminosity vs radio core luminosity at 5 GHz for the MAGN of Table 1. Blue squares (red open circles) correspond to possible FRI (FRII) classifications. The solid black line represents the calculated correlation as in Eq. 5. The light pink shaded area takes into account the 1σ error band in the derived correlation function.

From Table 1, the mean photon index Γ is 2.37, with spread 0.32. We notice that the power-law spectral slope is similar to the one of both blazars, 2.40 ± 0.02 (Abdo et al. 2010d), and the diffuse γ -ray background, 2.41 ± 0.05 (Abdo et al. 2010e). The γ -ray luminosity between energies ϵ_1 and ϵ_2 is given by:

$$L_\gamma(\epsilon_1, \epsilon_2) = 4\pi d_L^2(z) \frac{S_\gamma(\epsilon_1, \epsilon_2)}{(1+z)^{2-\Gamma}}, \quad (1)$$

where $d_L(z)$ is the luminosity distance at the redshift z and $S(\epsilon_1, \epsilon_2)$ is the observed energy flux between ϵ_1 and ϵ_2 . The factor $(1+z)^{2-\Gamma}$ is the so-called K-correction term that takes into account the redshift modification between the emitted and observed energies. The energy flux $S_\gamma(\epsilon_1, \epsilon_2)$ is linked to the photon flux $F_\gamma = \int_{\epsilon_1}^{\epsilon_2} d\epsilon dN/d\epsilon$ (in units of photons $\text{cm}^{-2} \text{s}^{-1}$) by the relation:

$$S_\gamma(\epsilon_1, \epsilon_2) = \int_{\epsilon_1}^{\epsilon_2} \epsilon \frac{dN}{d\epsilon} d\epsilon, \quad (2)$$

where $dN/d\epsilon$ is the γ -ray spectrum of the source.

Spectra for the sources in Table 1 have been taken from the 2FGL. They are simple power-law or log-parabola spectra:

$$\frac{dN}{d\epsilon} = \left(\frac{\epsilon}{\epsilon_{\text{pivot}}} \right)^{-\Gamma - \beta \log(\epsilon/\epsilon_{\text{pivot}})}, \quad (3)$$

the parameter β being zero for a power-law spectrum. Throughout the paper $\epsilon_1 = 0.1$ GeV, $\epsilon_2 = 100$ GeV, while ϵ_{pivot} has been varied for each source except when dealing with average properties ($\epsilon_{\text{pivot}} = 0.1$ GeV).

Radio luminosity is calculated for a fixed frequency following:

$$L_r(\nu) = \frac{4\pi d_L^2(z)}{(1+z)^{1-\alpha_r}} S_r(\nu) \quad (4)$$

where α_r is the radio spectral index (α_{core} or α_{tot}), $\Gamma = \alpha_r + 1$ and $S_r(\nu)$ is the radio energy flux at a given energy.

In Fig. 1 we plot the core radio and γ luminosities for the first 12 MAGN listed in Table 1. (The last three have been excluded from the sample as explained above). The possible classification into FRI and FRII RGs is also displayed. We

Table 1

Main radio and γ properties of the MAGN observed by *Fermi*-LAT. Column 1: name of the MAGN (radio classification: FRI or FRII), 2: redshift, 3: Galactic latitude, 4: spectral index for radio core (total) spectrum in a range including 5 GHz, 5: measured radio core (total) flux at 5 GHz; 6: photon index for γ -ray spectrum between 100 MeV - 100 GeV; 7- γ -ray flux above 100 MeV; 8- Radio core luminosity at 5 GHz; 9- γ -ray luminosity

References: 1-Morganti et al. (1993); 2-Pauliny-Toth et al. (1972); 3-Ekers et al. (1989); 4-Kuehr et al. (1981); 5-Spinrad et al. (1985); 6-Mullin et al. (2006); 7-Nagar et al. (2001); 8-Giovannini et al. (1988); 9-Laing et al. (1983); 10-Israel et al. (2008); 11-Burns et al. (1983); 12-Wright et al. (1994); 13-Evans et al. (2005); 14-Mantovani et al. (2009); 15-Jones et al. (2001); 16-Massardi et al. (2008); 17-Geldzahler & Fomalont (1984); 18-Becker et al. (1991); 19-Perley et al. (1997); 20-Linfield & Perley (1984); 21-Kadler et al. (2012); 22-Burgess & Hunstead (2006); 23-Kadler et al. (2012); 24-Gregory & Condon (1991)

MAGN(FRI,FRII)	z	b [$^\circ$]	$\alpha_{\text{core}}(\alpha_{\text{tot}})$	$S_{\text{core}}^{5\text{GHz}}$ [Jy] ($S_{\text{tot}}^{5\text{GHz}}$) [Jy]	Γ	F_γ [10^{-9} ph $\text{cm}^{-2} \text{s}^{-1}$]	$L_{r,\text{core}}^{5\text{GHz}}$ [erg s^{-1}]	L_γ [erg s^{-1}]
3C 78/NGC 1218(I)	0.0287	-44.6	0 (0.64 ¹)	0.964 \pm 0.164 ¹ (3.40 \pm 0.11 ²)	1.95 \pm 0.14	4.7 \pm 1.8	(8.8 \pm 1.4) \cdot 10 ⁴⁰	(1.11 \pm 0.54) \cdot 10 ⁴³
3C 274/M 87(I)	0.0038	74.5	0 (0.79 ⁸)	3.0971 \pm 0.0300 ⁷ (71.566 \pm 0.993 ⁹)	2.17 \pm 0.07	25.8 \pm 3.5	(4.90 \pm 0.05) \cdot 10 ³⁹	(6.2 \pm 1.1) \cdot 10 ⁴¹
Cen A(I)	0.0009	19.4	0.30 ¹⁰ (0.70 ¹⁰)	6.984 \pm 0.210 ¹¹ (62.837 \pm 0.099 ¹²)	2.76 \pm 0.05	175 \pm 10	(6.19 \pm 0.19) \cdot 10 ³⁸	(1.14 \pm 0.09) \cdot 10 ⁴¹
NGC 6251(I)	0.0247	31.2	0(0.72 ⁹)	0.38 \pm 0.04 ¹³ (0.510 \pm 0.050 ¹³)	2.20 \pm 0.07	18.2 \pm 2.6	(2.57 \pm 0.27) \cdot 10 ⁴⁰	(1.82 \pm 0.41) \cdot 10 ⁴³
Cen B(I)	0.0129	1.68	0 (0.13 ¹⁶)	2.730 ¹⁵ (6.58 \pm 1.04 ¹⁶)	2.33 \pm 0.12	39.3 \pm 11.4	5.02 \cdot 10 ⁴⁰	(8.6 \pm 3.2) \cdot 10 ⁴²
For A(I)	0.00587	-56.7	0.50 ¹⁷ (0.52 ¹)	0.051 ¹⁷ (72 ¹)	2.16 \pm 0.15	7.7 \pm 2.4	1.93 \cdot 10 ³⁸	(4.6 \pm 2.2) \cdot 10 ⁴¹
3C 120(I)	0.0330	-27.4	0 (0.44 ¹⁸)	3.458 \pm 0.588 ¹ (8.60 \pm 1.46 ¹)	2.71 \pm 0.35	29 \pm 17	(4.20 \pm 0.71) \cdot 10 ⁴¹	(2.9 \pm 1.6) \cdot 10 ⁴³
PKS 0625-35(I) ^b	0.0546	-20.0	0 (0.65 ³)	0.600 \pm 0.030 ³ (2.25 \pm 0.09 ⁴)	1.93 \pm 0.09	12.9 \pm 2.6	(2.02 \pm 0.10) \cdot 10 ⁴¹	(1.21 \pm 0.43) \cdot 10 ⁴⁴
Pictor A(II)	0.0351	-34.6	0 (1.07 ¹)	1.15 \pm 0.05 ¹⁹ (15.45 \pm 0.47 ⁴)	2.93 \pm 0.03	21.9 \pm 3.6	(1.58 \pm 0.07) \cdot 10 ⁴¹	(2.13 \pm 0.46) \cdot 10 ⁴³
3C 111(II)	0.0485	-8.61	-0.20 ^a (0.73 ⁵)	1.14 ²⁰ (6.637 \pm 0.996 ¹⁸)	2.54 \pm 0.19	40 \pm 8	2.98 \cdot 10 ⁴¹	(1.01 \pm 0.38) \cdot 10 ⁴⁴
3C 207(II) ^b	0.681	30.1	0 (0.90 ⁵)	0.5391 \pm 0.0030 ⁶ (1.35 \pm 0.04 ⁴)	2.36 \pm 0.11	17.3 \pm 3.3	(3.32 \pm 0.02) \cdot 10 ⁴³	(2.41 \pm 0.61) \cdot 10 ⁴⁶
3C 380(II) ^b	0.692	23.5	0 (0.71 ⁹)	5.073 \pm 0.105 ¹⁴ (7.45 \pm 0.37 ⁴)	2.34 \pm 0.07	30.3 \pm 3.7	(3.12 \pm 0.07) \cdot 10 ⁴⁴	(4.44 \pm 0.73) \cdot 10 ⁴⁶
IC 310(I)	0.0189	-13.7	n.a.(0.75 ²³)	n.a. (0.258 \pm 0.031 ²⁴)	2.10 \pm 0.19	11.1 \pm 6.2	-	(7.9 \pm 4.9) \cdot 10 ⁴²
3C 84/NGC 1275(I)	0.0176	-13.2	(0.78 ⁵)	high variability	2.00 \pm 0.02	175 \pm 8	-	(1.22 \pm 0.07) \cdot 10 ⁴⁴
PKS 0943-76(II)	0.270	-17.2	n.a.	upper limits(0.757 ²²)	2.44 \pm 0.14	19.5 \pm 5.1	-	(2.47 \pm 0.71) \cdot 10 ⁴⁵

^aour interpolation

^bnon-standard

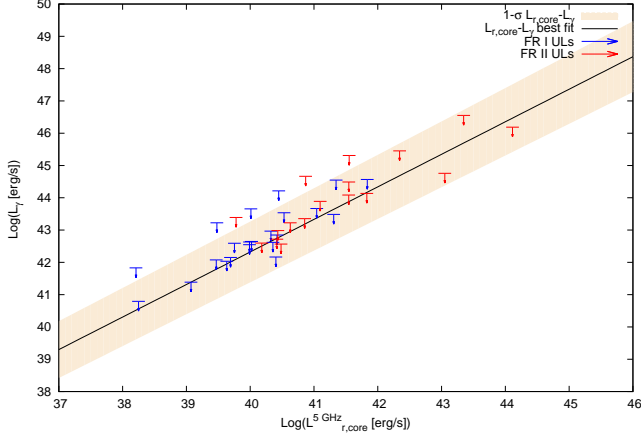


Figure 2. Upper limits on several *Fermi*-LAT undetected radio-loud MAGN. Blue (red) symbols refer to possible FRI (FRII) classification. The correlation in Eq. 5 (solid black line) is displayed together with the 1σ error band (light pink shaded area).

have calculated luminosities according to Eqs. 1-4, propagating errors on Γ while neglecting errors on the redshift, given their negligible effect. The correlation between $L_{r,core}$ and L_{γ} for the 12 objects is described by the function:

$$\log(L_{\gamma}) = 2.00 \pm 0.98 + (1.008 \pm 0.025) \log(L_{r,core}^{5\text{GHz}}), \quad (5)$$

represented by the solid line in Fig. 1, while the relevant 1σ error band is shown as a shaded area. It is obtained from the errors on both the γ -ray and radio luminosities, but the former dominates the uncertainty. Eq. 5 describes a linear correlation in the log-plane with a coefficient very close to one. γ -ray luminosities are greater than radio luminosities by about two orders of magnitude. The uncertainty band of the γ -ray fluxes measured by the *Fermi*-LAT spans one order of magnitude around the best fit. The significance of the correlation is tested in Sec.4.

It is useful to compare the $L_{r,core} - L_{\gamma}$ correlation obtained by removing three sources with non standard properties from the set of 12 MAGNs in Table 1. The radio morphology of 3C 380 is not unambiguously determined, as it shows some properties of a compact steep spectrum radio source (Abdo et al. 2010b; Wilkinson et al. 1991). The FRII 3C 207 behaves as a steep spectrum radio quasar in the optical band (Abdo et al. 2010b), while PKS 0625–35 has no clear association. We have therefore also calculated the correlation function excluding the galaxies 3C 380, 3C 207 and PKS 0625–35:

$$\log(L_{\gamma}) = 2.1 \pm 2.1 + (1.005 \pm 0.055) \log(L_{r,core}^{5\text{GHz}}). \quad (6)$$

The result is not very different from Eq. 5, if it were not for the increased spread in the fitted coefficients. Indeed, 3C 207 and PKS 0625–35 have large errors and 3C 380 is quite close to the correlation with the whole sample.

We report here also the correlation between the total radio luminosity at 5 GHz and the γ -ray luminosity for the whole sample of 12 sources. The correlation is found to be:

$$\log(L_{\gamma}) = -2.5 \pm 1.1 + (1.095 \pm 0.026) \log(L_{r,tot}^{5\text{GHz}}). \quad (7)$$

The experimental values for the total radio luminosity are quoted in Table 1. The fit for the sample of 9 sources results with:

$$\log(L_{\gamma}) = 3.5 \pm 2.3 + (0.948 \pm 0.056) \log(L_{r,tot}^{5\text{GHz}}). \quad (8)$$

9 sources The correlation implied by Eq. 5 is close to the one obtained in Ghisellini et al. (2005) for the very small sample of EGRET γ -ray loud FRI galaxies. In the case of blazars the slope of the correlation between $L_{\gamma} (> 100 \text{ MeV})$ and radio luminosity at different frequencies was found to be: 1.07 ± 0.05 at 20 GHz (Ghirlanda et al. 2010), 1.2 ± 0.1 at 5 GHz (Stecker et al. 1993) and 1.06 ± 0.02 at 8.4 GHz (Yuan & Wang 2012). The slope coefficient of the correlation for RGs is therefore similar to the correlation for blazars. This might indicate that the γ -ray emission mechanism is similar for MAGN and blazars. We therefore assume that the correlation in Eq. 5 is a good representation of the luminosity of the cores of MAGN and we will employ it in the remainder of this work in order to derive the emission of the MAGN population not detected by the *Fermi*-LAT, but potentially providing a non-negligible diffuse flux.

3. UPPER LIMITS FROM RADIO-LOUD FRI AND FRII GALAXIES NOT DETECTED BY *FERM*-LAT

In order to test the robustness of the core radio- γ correlation found in Eq. 5 we study a sample of radio-loud FRI and FRII galaxies that have not been detected by *Fermi*-LAT. For these objects we derive 95% C.L. γ -ray upper limits and verify that they are consistent with Eq. 5, given the uncertainty band shown in Fig. 1. The sample has been extracted from RGs in Kataoka et al. (2011) and Ghisellini et al. (2005) (first and second block in Table 2, respectively), and represents the sources with the highest radio core fluxes at 5 GHz. Further selection criteria have been applied in defining the sample for our purposes. From the sample of broad line RGs whose upper limits have been presented in Kataoka et al. (2011) we have excluded Pictor A (Brown & Adams 2012), detected in the meanwhile, and the sources that do not show a clear FRI or FRII radio morphology classification (RGB J1722+246 and PKS 2251+11 being Seyfert galaxies, S5 2116+81 being a flat spectrum radio source with a radio jet morphology). Moreover, sources with latitudes below 10° have been rejected in order to avoid a strong contamination from the Galactic plane foreground. This criterion applies to 4C 50.55 ($b = 0.39^\circ$). The same criteria have been applied to sources in Ghisellini et al. (2005) leading to the exclusion of 3C 84, 3C 274, 3C 78 already detected in γ rays, and 3C 75 that has an atypical RG morphology. Finally, 3C 317 has been excluded because of its variability (Venturi et al. 2004). Four FRII RGs from the 3CRR catalogue (3C 245, 3C 109, 3C 212, DA 240) have been added to the sample in order to cover a wider range in radio luminosity (last block in Table 2). Our sample is therefore composed of 17 FRII and 22 FRI RGs.

We have computed γ -ray flux upper limits for the listed galaxies by using the *Fermi*-LAT Science Tools¹. The data taking period for the analysis is from the starting time of the mission, 2008 August 4, until 2012 September 9. The Mission Elapsed Time (MET) interval runs from 239557414 to 368928003. Data have been extracted from a region of interest (ROI) of radius = 8° centered at the position of the source. This radius represents the best angular region for source analysis as long as sources are far from the Galactic plane (Abdo et al. 2009b), and indeed we neglect in this analysis sources that lie below 10° in latitude. We selected γ -rays in the energy range 100 MeV - 100 GeV.

¹ <http://fermi.gsfc.nasa.gov/ssc/data/analysis/documentation>, software version v9r27p1, Instrumental Response Functions (IRFs) P7-V6

We are using P7SOURCE_V6 photons. Good survey data are selected accordingly to software recommendations, with the rocking angle selected to be less than 52° . Data selection and preparation eliminate photons from the Earth limb by applying a cut on the zenith angle of 100° . An unbinned maximum-likelihood analysis was performed. In the cases where the fit did not converge we have performed a binned analysis as recommended. We therefore analyze the source region with both methods and draw the upper limits with the help of the LATAnalysisScripts², which make use of the UpperLimits.py module.

Each galaxy in the sample was modeled as a point-like source with a power-law spectrum of index $\Gamma = 2.5$. This value has been chosen as nominal spectral index for all MAGN in analogy with Kataoka et al. (2011). We have verified that choosing $\Gamma = 2.3$, closer to the distribution of the spectral indices from 1 changes the limits by $\sim 10\%$, while an index of 2.7 leaves results unchanged. The number of expected counts in the ROI is derived by considering the emission from all sources in the 2FGL³ inside a source region (distance from the target region) of 13° ($8^\circ + 5^\circ$). The fitting procedure leaves the spectral parameters of all the sources inside the ROI free, whereas sources in the region $8^\circ < r < 13^\circ$ have spectral parameters fixed to the values of the 2FGL. Additional backgrounds are the Galactic diffuse emission and the isotropic diffuse model, which includes the true IGRB and the residual particle contamination⁴. The diffuse models used in the analysis are: gal_2yearp7v6_v0.fits for the Galactic diffuse model and iso_p7v6source.txt for the isotropic spectral template. All the relevant normalizations have been left as free parameters during the fitting procedure. The method used to compute the upper limits is a standard profile likelihood. A 95% upper limit (UL) has been computed when the Test Statistic (TS) was less than 25. In Table 2 the flux upper limits are quoted together with the TS value for both unbinned and binned analysis. Given the systematic uncertainty arising from the different statistical methods, we adopt as *upper* limit the highest value for the flux bound. These *conservative* upper limits are shown in Fig. 2 with the luminosity correlation from Eq. 5 overlaid. It is evident that the calculated upper limits do not fall below the uncertainty band, thus corroborating our core radio and γ -ray correlation.

4. TEST OF THE RADIO- γ CORRELATION

The correlation established in Eq. 5 could be biased by distance dependence of the luminosity and flux-limited samples. We have tested the strength of the correlation via a partial correlation analysis, in order to verify that the radio core - γ -ray luminosity correlation for MAGN is not spurious.

Firstly, we calculate the Spearman rank-order correlation coefficient. The Spearman correlation coefficients are 0.94, 0.92, 0.98 between $\log(L_{r,\text{core}}^{5\text{GHz}})$ and $\log(L_\gamma)$, between $\log(L_{r,\text{core}}^{5\text{GHz}})$ and redshift, and between $\log(L_\gamma)$ and redshift, respectively. The partial correlation coefficient turns out to be 0.51 and the null hypothesis that the two luminosities are uncorrelated is rejected at the 95% C.L.

Moreover, we test the significance of the radio- γ correlation by using the modified Kendall τ rank correlation test proposed by Akritas & Siebert (1996), which is suitable for partially-

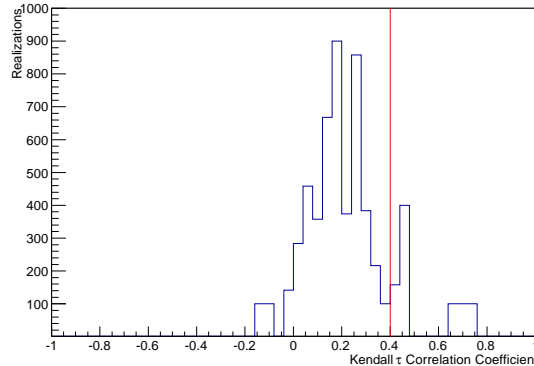


Figure 3. Null hypothesis distribution of τ correlation coefficients assuming independence between the γ and radio wavebands. The null hypothesis distributions are generated from 5800 permutations of γ -ray luminosities among the galaxies by requiring that the resultant γ -ray fluxes exceed the flux threshold of $7.7 \cdot 10^{-9}$ photons $\text{cm}^{-2} \text{s}^{-1}$. The mean value is 0.223 with the standard deviation of the distribution RMS=0.173. The correlation coefficient of the actual data is represented by the red solid line, $\tau = 0.397$.

censored datasets. By following the procedure highlighted in Ackermann et al. (2012a), we perform a Monte Carlo simulation in order to compute the distribution of the τ correlation coefficients obtained under the null hypothesis of independence between the two wavebands. Starting from the detected sample of 12 sources we build several dataset realizations by scrambling the derived γ -ray luminosities among galaxies. For each galaxy we then compute the corresponding flux and we retain only galaxies with a flux above the minimal γ -ray flux of the detected sample ($7.7 \cdot 10^{-9}$ photons $\text{cm}^{-2} \text{s}^{-1}$). If the scrambled sample has fewer than 12 sources above the flux threshold, we randomly extract an additional source from the upper limit dataset (from Table 2) until the flux threshold is reached. For each scrambled dataset we then compute the Kendall coefficient and we build its distribution as shown in Fig. 3. The displayed distribution refers to 5800 realizations of scrambled samples and the red line represents the value of the τ correlation coefficient of the actual data, $\tau = 0.397$.

Finally, we compare the τ correlation coefficient of the actual data to the distribution of τ and we find that the integral of the distribution above $\tau = 0.397$ is 0.05. This is the probability to obtain the actual correlation by chance, *i.e.* the p-value of the correlation (the smaller the p-value, the greater the probability for the observed correlation of being true). As in the case of the Spearman test, we can exclude the correlation happening by chance at the 95% C.L. The result indicates a physical correlation between the core radio emission and the γ -ray flux of the *Fermi*-LAT detected MAGN.

5. THE γ -RAY LUMINOSITY FUNCTION

The luminosity function for a given energy defines the number of sources emitting at that energy per unit comoving volume, per unit (base 10) logarithm of luminosity:

$$\rho(L, z) = \frac{d^2 N}{d \log(L) dV}. \quad (9)$$

In the radio band, data are available for hundreds of radio-loud MAGN, depending on the frequency of the survey. Usually radio observations refer to the total emission of the AGN, including the central region, jets and radio lobes. Only for a limited number of objects detected at low radio frequencies

² User contributions <http://fermi.gsfc.nasa.gov/ssc/data/analysis/user/>

³ http://fermi.gsfc.nasa.gov/ssc/data/access/lat/2yr_catalog/

⁴ <http://fermi.gsfc.nasa.gov/ssc/data/access/lat/BackgroundModels.html>

Table 2

Flux upper limits on a sample of MAGN. Column 1: name of the MAGN (radio classification: FRI or FR II), 2: redshift, 3: measured radio core flux at 5 GHz [Jy], 4: TS of unbinned analysis, 5: 95% C.L. upper limit from unbinned analysis on the flux above 100 MeV in units of 10^{-9} ph cm $^{-2}$ s $^{-1}$, 6: TS of binned analysis, 7: 95% C.L. upper limit from binned analysis on the flux above 100 MeV in units of 10^{-9} ph cm $^{-2}$ s $^{-1}$; 8: radio core luminosity at 5 GHz in units of erg s $^{-1}$.

References: 1-Morganti et al. (1993); 2-Henstock et al. (1995); 3-Third Cambridge Catalogue of Radio Sources ; 4-Dodson et al. (2008); 5-Neff et al. (1995); 6-Pearson et al. (1992); 7-Tingay et al. (2002).

MAGN(FRI,FR II)	z	$S_{5\text{GHz}}^{\text{core}}$ [Jy]	$\text{TS}_{\text{unbinned}}$	$F_{\text{unbinned}}^{\text{OL}}$	$\text{TS}_{\text{binned}}$	$F_{\text{binned}}^{\text{OL}}$	$L_{r,\text{core}}^{5\text{GHz}}$
3C 18 (II)	0.188	0.083 ¹	< 1	2.7	2.6	6.0	$3.51 \cdot 10^{41}$
B3 0309+411B (II)	0.134	0.320 ²	-	-	< 1	5.8	$6.73 \cdot 10^{41}$
3C 215 (II)	0.412	0.0164 ³	< 1	3.1	4.1	6.0	$3.56 \cdot 10^{41}$
3C 227 (II)	0.086	0.032 ¹	< 1	0.1	< 1	1.1	$2.70 \cdot 10^{40}$
3C 303 (II)	0.141	0.150 ³	< 1	2.8	3.3	4.6	$3.50 \cdot 10^{41}$
3C 382 (II)	0.058	0.188 ³	< 1	4.1	1.2	5.9	$7.12 \cdot 10^{40}$
3C 390.3 (II)	0.056	0.120 ⁴	< 1	1.7	3.0	4.7	$4.26 \cdot 10^{40}$
3C 411(II)	0.467	0.078 ⁵	-	-	< 1	6.1	$2.2 \cdot 10^{42}$
4C 74.26 (II)	0.104	0.100 ⁶	1.1	5.4	< 1	5.7	$1.25 \cdot 10^{41}$
PKS 2153-69 (II)	0.028	0.300 ⁷	4.2	6.6	< 1	6.2	$2.67 \cdot 10^{40}$
3C 445 (II)	0.056	0.086 ¹	< 1	0.8	< 1	1.0	$3.06 \cdot 10^{40}$
3C 465 (I)	0.029	0.270 ³	-	-	< 1	0.5	$2.5 \cdot 10^{40}$
3C 346 (I)	0.162	0.220 ³	4.5	6.4	10.8	10.2	$1.39 \cdot 10^{39}$
3C 264 (I)	0.021	0.200 ³	9.0	5.7	14.0	7.5	$9.58 \cdot 10^{39}$
3C 66B (I)	0.022	0.182 ³	-	-	< 1	8.3	$9.31 \cdot 10^{39}$
3C 272.1(I)	0.003	0.180 ³	5.2	5.6	5.3	6.8	$1.66 \cdot 10^{38}$
3C 315 (I)	0.1083	0.150 ³	-	-	< 1	2.1	$2.04 \cdot 10^{41}$
3C 338 (I)	0.030	0.105 ³	-	-	< 1	4.6	$1.07 \cdot 10^{40}$
3C 293 (I)	0.045	0.100 ¹	< 1	1.5	< 1	1.8	$2.29 \cdot 10^{40}$
3C 29 (I)	0.045	0.093 ³	< 1	1.5	< 1	4.1	$2.11 \cdot 10^{40}$
3C 31(I)	0.017	0.092 ³	-	-	< 1	4.0	$2.83 \cdot 10^{39}$
3C 310 (I)	0.054	0.080 ³	< 1	1.2	< 1	2.1	$2.63 \cdot 10^{40}$
3C 296 (I)	0.024	0.077 ³	< 1	1.5	< 1	2.3	$4.79 \cdot 10^{39}$
3C 89 (I)	0.1386	0.049 ³	-	-	< 1	1.8	$1.10 \cdot 10^{41}$
3C 449 (I)	0.017	0.037 ³	< 1	0.5	< 1	0.8	$1.19 \cdot 10^{39}$
3C 288 (I)	0.246	0.030 ³	< 1	1.5	1.6	3.7	$2.22 \cdot 10^{41}$
3C 305 (I)	0.0414	0.0295 ³	-	-	< 1	2.1	$5.66 \cdot 10^{39}$
3C 83.1B (I)	0.026	0.040 ³	10.0	19.7	16.5	23.2	$2.89 \cdot 10^{39}$
3C 424 (I)	0.1270	0.0180 ³	-	-	< 1	1.6	$3.39 \cdot 10^{40}$
3C 438 (II)	0.290	0.0071 ³	< 1	0.9	< 1	3.2	$7.40 \cdot 10^{40}$
3C 386 (I)	0.018	0.120 ³	-	-	< 1	3.2	$4.15 \cdot 10^{39}$
3C 277.3 (I)	0.0857	0.0122 ³	-	-	4.2	5.1	$1.03 \cdot 10^{40}$
3C 348 (I)	0.1540	0.010 ³	-	-	< 1	5.1	$2.80 \cdot 10^{40}$
3C 433 (II)	0.102	0.005 ³	-	-	< 1	1.9	$5.96 \cdot 10^{39}$
3C 442A (I)	0.027	0.002 ³	< 1	0.7	< 1	0.9	$1.62 \cdot 10^{38}$
3C 245 (II)	1.029	0.910 ³	< 1	2.0	< 1	4.0	$1.30 \cdot 10^{44}$
3C 109 (II)	0.306	0.263 ³	< 1	1.4	< 1	3.5	$3.06 \cdot 10^{42}$
3C 212 (II)	1.049	0.150 ³	6.4	7.1	10.11	8.8	$2.22 \cdot 10^{43}$
da 240 (II)	0.036	0.105 ³	< 1	1.5	< 1	2.8	$1.48 \cdot 10^{40}$

(around 0.1-few GHz), the flux from the central core alone has been measured. The RLF is derived phenomenologically by fitting data on the emission of the radio sample. Results on the total RLF are quite well established (Willott et al. 2001; Dunlop & Peacock 1990; Yuan & Wang 2012), while the literature about the core radio luminosity function is still limited (Yuan & Wang 2012), given the scarcity of experimental data.

Unfortunately, deriving the GLF from fitting the gamma-ray measurements is not feasible, due to the small size of the γ -ray loud MAGN sample. Following previous attempts applied to blazars (Stecker & Salamon 1996; Kazanas & Perlman 1997; Narumoto & Totani 2006; Inoue & Totani 2009; Abazajian et al. 2011; Stecker & Venters 2011) and, to a lesser extent, to RGs (Ghisellini et al. 2005; Inoue 2011), we derive the GLF from the RLF by exploiting the correlation between radio and

γ -ray luminosities found in Sect. 2. We assume that:

$$N_{\gamma} = k N_r, \quad (10)$$

where the normalization k takes into account our ignorance of the number of radio-loud MAGN emitting in γ rays as well (N_r and N_{γ} , respectively). From Eq. 9, it follows that $N = \int dV \int \rho(L, z) d \log L$ and therefore the GLF is defined through a RLF by:

$$\rho_{\gamma}(L_{\gamma}, z) = k \rho_r(L_r, z) \frac{d \log L_r}{d \log L_{\gamma}}. \quad (11)$$

Given the results of the previous sections, the above equation

takes the specific form:

$$\rho_\gamma(L_\gamma, z) = k \rho_{r,\text{core}}(L_{r,\text{core}}^{5\text{GHz}}(L_\gamma), z) \frac{d \log L_{r,\text{core}}^{5\text{GHz}}(L_\gamma)}{d \log L_\gamma}, \quad (12)$$

where $\rho_{r,\text{core}}$ refers to the radio luminosity function of the cores of the MAGN. If our hypothesis of a correlation between the core radio and γ emission is physical, as supported by the results on the ULs (see previous section), we might expect k values not too far from 1. In other words, each RG with a bright radio core is expected to emit in the γ -ray band as well. The correlation between radio and γ -ray luminosities is assumed to be a specific analytical expression, Eq. 5, shown to be in very good agreement with the data. In this sense, the scatter in the correlation derives only from errors in the experimental data and not in a potential scatter on the luminosity form. The radio luminosity is energetically weaker, according to Eq. 5. As already noted, the lack of a reliable core RLF from data prevents us from using Eq.12 directly. We will therefore make use of the total RLF and obtain the core RLF through the link between total and core radio luminosities.

As a first ingredient, we need a correlation between radio core and total luminosities. In Fig.4 we display the correlation between $L_{\nu,\text{tot}}^{5\text{GHz}}$ and $L_{\nu,\text{core}}^{5\text{GHz}}$. The three curves correspond to:

$$\log L_{\nu,\text{core}}^{5\text{GHz}} = 4.2 \pm 2.1 + (0.77 \pm 0.08) \log L_{\nu,\text{tot}}^{1.4\text{GHz}} \quad (13)$$

from Lara et al. (2004) (black solid curve),

$$\log L_{\nu,\text{core}}^{5\text{GHz}} = 7.6 \pm 1.1 + (0.62 \pm 0.04) \log L_{\nu,\text{tot}}^{408\text{MHz}} \quad (14)$$

from Giovannini et al. (2001) (pink dot-dashed curve),

$$\log L_{\nu,\text{tot}}^{408\text{MHz}} = 7.10 \pm 0.90 + (0.83 \pm 0.04) \log L_{\nu,\text{core}}^{5\text{GHz}} \quad (15)$$

from Yuan & Wang (2012) (green dotted curve). We report all the luminosities at 5 GHz, assuming a power-law dependence $L/\nu \propto \nu^{-\alpha}$, with $\alpha_{\text{tot}} = 0.80$. It is clear from Fig. 4 that the experimental data for our MAGN sample are best represented by the correlation proposed by Lara et al. (2004). We will therefore adopt Eq.13 throughout the paper. The possible systematics introduced by this correlation are likely compensated, at least to a good extent, by the fit to the cumulative number counts (see the following section).

The core RLF may be obtained from the total one following the same reasoning as for Eqs. 10-11:

$$\rho_{r,\text{core}}(L_{r,\text{core}}, z) = \rho_{r,\text{tot}}(L_{r,\text{tot}}, z) \frac{d \log L_{r,\text{tot}}}{d \log L_{r,\text{core}}}, \quad (16)$$

where we expect that the number of MAGN showing core and total emission is almost the same. We adopt as the total RLF the one derived in Willott et al. (2001) (Model C with $\Omega_M=0$) and shift luminosities from 151 MHz to 5 GHz according to the power law explained above. We convert the comoving volume to the standard Λ CDM cosmology by using the conversion factor $\eta(z)$:

$$\eta(z) = \frac{d^2 V_W / dz d\Omega}{d^2 V / dz d\Omega}, \quad (17)$$

where $d^2 V_W / dz d\Omega$ is the comoving volume element used by Willott et al. (2001):

$$\frac{d^2 V_W}{dz d\Omega} = \frac{c^3 z^2 (2+z)^2}{4H_{0,W}^3 (1+z)^3}, \quad (18)$$

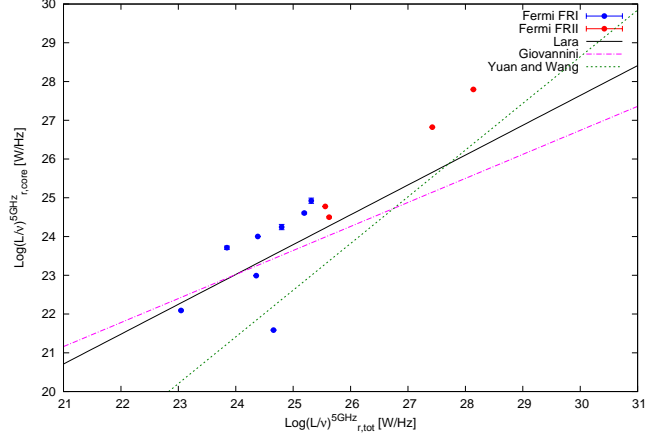


Figure 4. Radio core luminosity versus total radio luminosity at 5 GHz. Solid black line corresponds to Eq. 13, while the pink dot-dashed and the green dotted correspond to Eq.14 and Eq.15, respectively. Blue squares (red open circles) are the experimental data for our sample of FRI (FRII) taken from Table 1.

c is the speed of light and $H_{0,W} = 50 \text{ km s}^{-1} \text{ Mpc}^{-1}$. In the cosmological model Λ CDM the comoving volume element is defined as:

$$\frac{d^2 V}{dz d\Omega} = \frac{c d_L(z)^2}{H_0 (1+z)^2 \sqrt{(1-\Omega_\Lambda - \Omega_M)(1+z)^2 + (1+z)^3 \Omega_M + \Omega_\Lambda}}. \quad (19)$$

We finally obtain the GLF inserting Eq.16 in Eq.12:

$$\rho_\gamma(L_\gamma, z) = k \rho_{r,\text{tot}}(L_{r,\text{tot}}^{5\text{GHz}}(L_{r,\text{core}}^{5\text{GHz}}(L_\gamma)), z) \cdot \frac{d \log L_{r,\text{core}}^{5\text{GHz}}}{d \log L_\gamma} \frac{d \log L_{r,\text{tot}}^{5\text{GHz}}}{d \log L_{r,\text{core}}^{5\text{GHz}}}. \quad (20)$$

The $d \log L_{r,\text{core}}^{5\text{GHz}} / d \log L_\gamma$ will be computed from Eq.5, while the $d \log L_{r,\text{tot}}^{5\text{GHz}} / d \log L_{r,\text{core}}^{5\text{GHz}}$ derives from the total-core correlation, Eq.13.

6. PREDICTIONS FOR THE SOURCE COUNT DISTRIBUTION

An important observable for the correctness of our method is provided by the source count distribution of MAGN measured by *Fermi*-LAT. The source count distribution, known also as $\log N - \log S$, is the cumulative number of sources $N(> F_\gamma)$ detected above a threshold flux F_γ . We have derived the experimental source count distribution of the 12 MAGN of our sample following (Abdo et al. 2010e):

$$N(> F_\gamma) = \sum_{i=1}^{N(>F_{\gamma,i})} \frac{1}{\omega(F_{\gamma,i})}, \quad (21)$$

where the sum runs on all the i -sources with a γ -ray flux $F_{\gamma,i} > F_\gamma$, and $\omega(F_{\gamma,i})$ is the flux dependent detection efficiency compatible with our sample. As shown in Abdo et al. (2009a, 2010e), at faint fluxes the *Fermi*-LAT more easily detects hard-spectrum sources rather than sources with a soft spectrum. Sources with a photon index of $\Gamma=1.5$ can be detected down to fluxes that are a factor > 20 fainter than those of a source with a photon index of 3.0. Given this strong selection effect, the intrinsic photon-index distribution is necessarily different from the observed one. This effect is taken

into account by the detection efficiency. Since the latter is not available for the MAGN sample, we reasonably assume it is the same as for blazars and take it from Abdo et al. (2010d). The theoretical source count distribution $N_{\text{th}}(> F_\gamma)$ for a γ -ray flux F_γ is calculated following the definition of GLF in Eq. 9:

$$N_{\text{th}}(> F_\gamma) = 4\pi \int_{\Gamma_{\text{min}}}^{\Gamma_{\text{max}}} \frac{dN}{d\Gamma} d\Gamma \int_0^{z_{\text{max}}} \frac{d^2V}{dzd\Omega} \int_{L_\gamma(F_\gamma, z, \Gamma)}^{L_\gamma^{\text{max}}} \frac{dL_\gamma}{L_\gamma \ln(10)} \rho_\gamma(L_\gamma, z, \Gamma), \quad (22)$$

where $L_\gamma(F_\gamma, z, \Gamma)$ is the γ -ray luminosity of a RG at redshift z , whose photon spectral index is Γ and photon flux is F_γ (integrated above 100 MeV). The spectral index distribution, $dN/d\Gamma$, is assumed to be gaussian in analogy with blazars (Abdo et al. 2010d). The comoving volume, $d^2V/(dzd\Omega)$, is computed according to Eq.19. We fix $\Gamma_{\text{min}}=1.0$, $\Gamma_{\text{max}}=3.5$, $z_{\text{max}} = 6$ and $L_{\gamma, \text{max}} = 10^{50} \text{ erg s}^{-1}$.

Fig. 5 shows the theoretical $N_{\text{th}}(> F_\gamma)$, calculated from Eq.22, with several bands of uncertainty, overlaid with the experimental source count distribution from Eq.21. Their comparison is discussed here only as a consistency check of the validity of the assumptions involved in Eq.22 and in particular of the ratio of MAGN emitting in γ rays relative to those emitting in radio-core, i.e. the k parameter in Eq. 22. The data points for the experimental $N(> F_\gamma)$ are in fact highly correlated, and a fit to those points is not statistically meaningful. Nonetheless, it is useful to fit the theoretical $N_{\text{th}}(> F_\gamma)$ to the experimental source count distribution to constrain the only free parameter k in this calculation. Additionally, the shape of the function predicting $N(> F_\gamma)$ is essentially driven by the radio luminosity density function, and not by the fit to the experimental source count distribution.

The black dashed line in Fig. 5 has been derived from the best fit parameters of the $L_{r, \text{core}} - L_\gamma$ correlation (namely Eq.5), whose fit to the experimental source count distribution gives $k = 3.05$. This indicates that the best fit radio core- γ correlation function slightly under-predicts the distribution of MAGN observed by *Fermi*-LAT.

For obtaining the bands depicted in Fig. 5, we have proceeded as follows:

- i) we have calculated the $N(> F_\gamma)$ for all the correlation coefficients falling in the 1σ uncertainty band for the $L_{r, \text{core}} - L_\gamma$ relationship (Fig. 1);
- ii) for each combination of these coefficients we have determined k from the comparison with the $\log N - \log S$ (pink shaded area);
- iii) the configuration with the lowest χ^2 among all the configurations explored at point ii predicts the best $N(> F_\gamma)$ (black solid line, $k=0.258$);
- iv) all the configurations giving a 1σ variation from the lowest χ^2 (minimal $\chi^2 + 3.53$) span the cyan shaded area.

The red dot-dashed curve was obtained for the radio total - γ -ray luminosity correlation in Eq.7 and the total RLF in Willott et al. (2001). This hypothesis leads to a lower number of sources at the lowest fluxes.

Finally, the green shaded band was obtained by fixing the normalization factor k in Eqs. 10,11 equal to 1, which represents the ideal situation in which we predict that each MAGN has a radio-loud central region emitting in γ rays as well. This result is an important test of the validity of our initial assumption that a MAGN with a radio core emission also emits pho-

tons in the γ -ray energy band, via likely SSC and EC processes. It is remarkable that the band is a good fit to *Fermi*-LAT data.

Given the uncertain classification of some of the sources, as explained in Sec.2, we also provide the source count distribution for the 9 sources with firm FRI or FRII classification, Fig.6. We show the experimental and the theoretical source count distribution predicted when the three galaxies 3C 380, 3C 207 and PKS 0625-35 are excluded from the analysis. The black solid line is the same as in Fig. 5, but obtained with 9 data points and employing Eq. 6 for the $L_{r, \text{core}} - L_\gamma$ luminosity correlation function. The result is compatible with data, with $\chi^2 = 4.65$ and the normalization for the source number distribution $k=2.37$. The red dot-dashed curve is the same as in Fig. 5, but obtained from the total RLF and Eq.8, and minimized with respect to the 9 data points.

7. THE DIFFUSE γ -RAY EMISSION FROM MAGN

The diffuse γ -ray flux due to the whole population of MAGN may be estimated as follows:

$$\frac{d^2F(\epsilon)}{d\epsilon d\Omega} = \int_{\Gamma_{\text{min}}}^{\Gamma_{\text{max}}} d\Gamma \frac{dN}{d\Gamma} \int_0^{z_{\text{max}}} \frac{d^2V}{dzd\Omega} \int_{L_{\gamma, \text{min}}}^{L_{\gamma, \text{max}}} \frac{dF_\gamma}{d\epsilon} \cdot \frac{dL_\gamma}{L_\gamma \ln(10)} \rho_\gamma(L_\gamma, z) (1 - \omega(F_\gamma(L_\gamma, z))) \exp(-\tau_{\gamma, \gamma}(\epsilon, z)). \quad (23)$$

The minimum γ -ray luminosity value is set to $10^{41} \text{ erg s}^{-1}$, the maximum at $10^{50} \text{ erg s}^{-1}$. The term $\omega(F_\gamma(L_\gamma, z))$ is the detection efficiency of *Fermi*-LAT at the photon flux F_γ , which corresponds to the flux from a source with a γ -ray luminosity L_γ at redshift z . $dN/d\Gamma$ is the photon spectral index distribution (see Eq.22). $dF_\gamma/d\epsilon$ is the intrinsic photon flux at energy ϵ , for a MAGN with γ -ray luminosity L_γ (Venters et al. 2009; Yan et al. 2012):

$$\frac{dF_\gamma}{d\epsilon} = \frac{(1+z)^{2-\Gamma}}{4\pi d_L(z)^2} \frac{(2-\Gamma)}{\left[\left(\frac{\epsilon}{\epsilon_1} \right)^{2-\Gamma} - 1 \right]} \left(\frac{\epsilon}{\epsilon_1} \right)^{-\Gamma} \frac{L_\gamma}{\epsilon_1^2}. \quad (24)$$

High-energy γ rays ($\epsilon > 20 \text{ GeV}$) propagating in the Universe are absorbed by the interaction with the extragalactic background light (EBL), cosmic optical radiation and infrared background (Salamon & Stecker 1998; Stecker et al. 2006; Mazin & Raue 2007; Razzaque et al. 2009; Gilmore et al. 2009; Finke et al. 2010; Ackermann et al. 2012b), with an optical depth $\tau_{\gamma, \gamma}(\epsilon, z)$. In this study we adopt the attenuation model of Finke et al. (2010). The γ -ray absorption creates electron-positron pairs, which can scatter off the CMB photons yielding a secondary cascade emission at the γ -ray energies. However, we do not take into account the cascade emission because the contribution is expected to be negligible for soft sources like MAGN (Venters 2010). Fig.7 shows the diffuse γ -ray flux due to the MAGN population as a function of γ -ray energy, along with the *Fermi*-LAT data for the IGRB (Abdo et al. 2010c). The cyan shaded area derives from the 1σ uncertainty band on the $L_{r, \text{core}} - L_\gamma$ correlation and on the k parameter in the source count distribution (see description of the cyan shaded area in Fig. 5). The upper edge of the uncertainty band skims the IGRB data points, while the lower limit is almost an order of magnitude below the data. The band itself is nearly a factor of ten wide. The flux integrated above 100 MeV is $5.69 \cdot 10^{-7} \text{ cm}^{-2} \text{ s}^{-1} \text{ sr}^{-1}$ for the lower bound of the uncertainty band, and $4.91 \cdot 10^{-6} \text{ cm}^{-2} \text{ s}^{-1} \text{ sr}^{-1}$

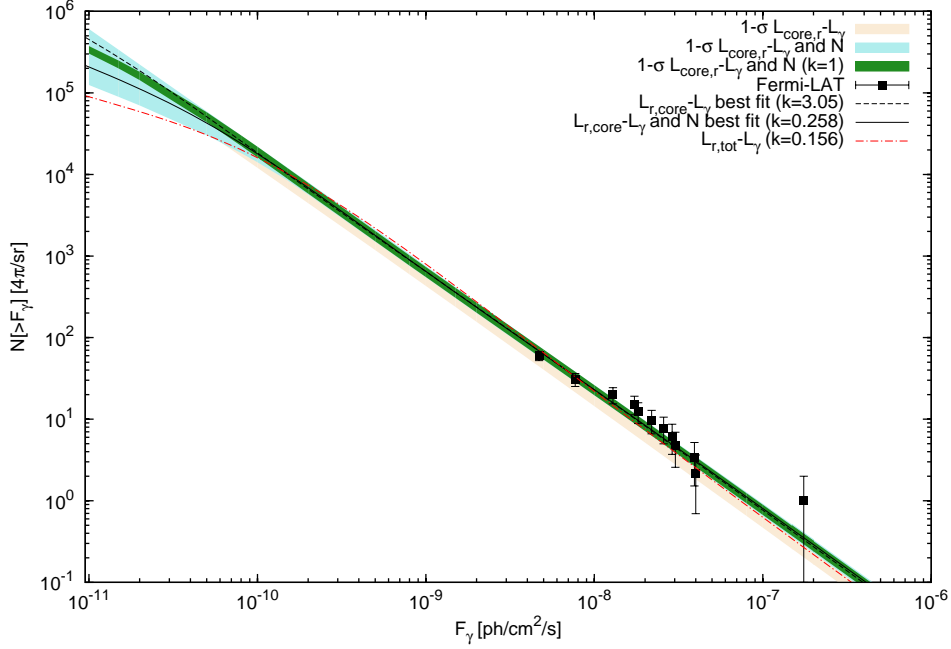


Figure 5. Source count distribution as a function of the integrated γ -ray flux. *Fermi*-LAT data are represented by black squares with 1σ error bars. The black dashed line (pink shaded area) shows the source count distribution predicted with the best fit configuration (1σ uncertainty band) for the $L_{r,\text{core}} - L_\gamma$ correlation in Eq.5 (Fig. 1). The black solid line (cyan shaded area) corresponds to the source count distribution predicted after the minimization on the $L_{r,\text{core}} - L_\gamma$ best fit (1σ uncertainty band) correlation and k (see text for details). The green shaded area includes all the configurations with $k=1$. The red dot-dashed curve has been obtained with the $L_{r,\text{tot}} - L_\gamma$ correlation according to Eq.7.

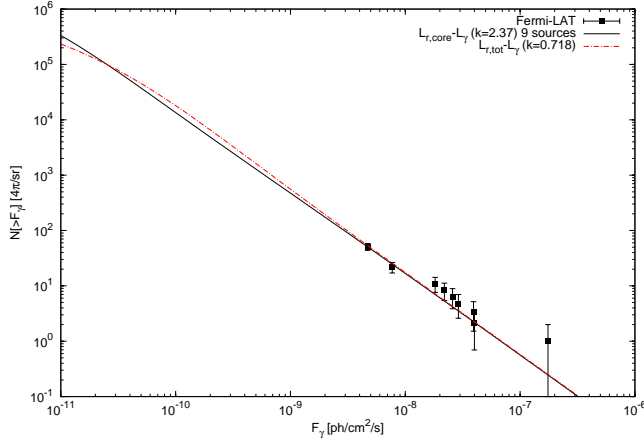


Figure 6. Source count distribution as a function of the integrated γ -ray flux for 9 RGs. *Fermi*-LAT data are represented by black squares with 1σ error bars. The black solid line corresponds to the source count distribution predicted with the best fit configuration for the $L_{r,\text{core}} - L_\gamma$ correlation in Eq. 6 and $N(> F_\gamma)$. The red dot-dashed curve has been obtained with the $L_{r,\text{tot}} - L_\gamma$ correlation according to Eq.8.

for the upper one. These values compare with $1.03 \cdot 10^{-5} \text{ cm}^{-2} \text{ s}^{-1} \text{ sr}^{-1}$ derived from the experimental data (Abdo et al. 2010c). The green band has been obtained by fixing $k = 1$ as described in Sect. 6 on Fig. 5. It corresponds to the case in which all the MAGN with a radio-loud central region emit in γ rays as well, and with a phenomenological model that fits nicely all the experimental constraints.

The flux calculated for the best fit coefficients of the $L_{r,\text{core}} - L_\gamma$ correlation and $k=3.05$ (see description of the black dashed line in Fig. 5) is displayed as the black dashed line in Fig. 7. Our predictions are for a MAGN population whose γ -ray emission is assumed to originate from the central region of the active galaxy, and modeled from the core RLF.

The dot-dashed red line represents the flux derived when the γ -ray luminosity is correlated with the total radio luminosity according to Eq. 7, and total RLF (Willott et al. 2001) (see description of the red dot-dashed line in Fig. 5). The effect of EBL absorption is clear from the softening of the flux above 50 GeV. The deviation from a pure power-law shape below ~ 30 GeV is due to integration over the photon index distribution. We note that the contribution of unresolved blazars (Abdo et al. 2010d) has a very similar slope but is lower than the one obtained for MAGN in this paper. The two uncertainty bands nearly touch each other.

The flux displayed in Fig. 7 results from an integration up to a maximum luminosity of $10^{50} \text{ erg s}^{-1}$. The result does not depend on the maximal luminosity of integration, confirming that the photons come from very numerous and very faint sources. A confirmation of the negligible contribution of bright sources to the overall flux is that the flux at 1 GeV (multiplied by E^2) for the 15 galaxies of Table 1 is $3.5 \cdot 10^{-6} \text{ MeV cm}^{-2} \text{ s}^{-1} \text{ sr}^{-1}$, more than two orders of magnitude below our estimated diffuse flux. We finally observe that shifting the lower luminosity from $10^{41} \text{ erg s}^{-1}$ down to $10^{38} \text{ erg s}^{-1}$ would lead to a 15% greater isotropic intensity.

Our predictions may be compared to the results reported by Inoue (2011). In that paper, the flux from unresolved MAGN has been obtained for a single model, which is contained in our uncertainty band and shows a different shape with respect to our representative cases (solid and dashed lines in Fig. 7). Possible differences between the two procedures are probably due to the fact that Inoue (2011) works within a smaller and different RG sample. We both establish a $L_{r,\text{core}} - L_\gamma$ correlation. However, we convert the total RLF by Willott et al. (2001) to core RLF, while Inoue (2011) does not make this transformation. Data on the source number distribution are different, in particular the *Fermi*-LAT data points at the lowest fluxes. A final possible difference might reside in a dif-

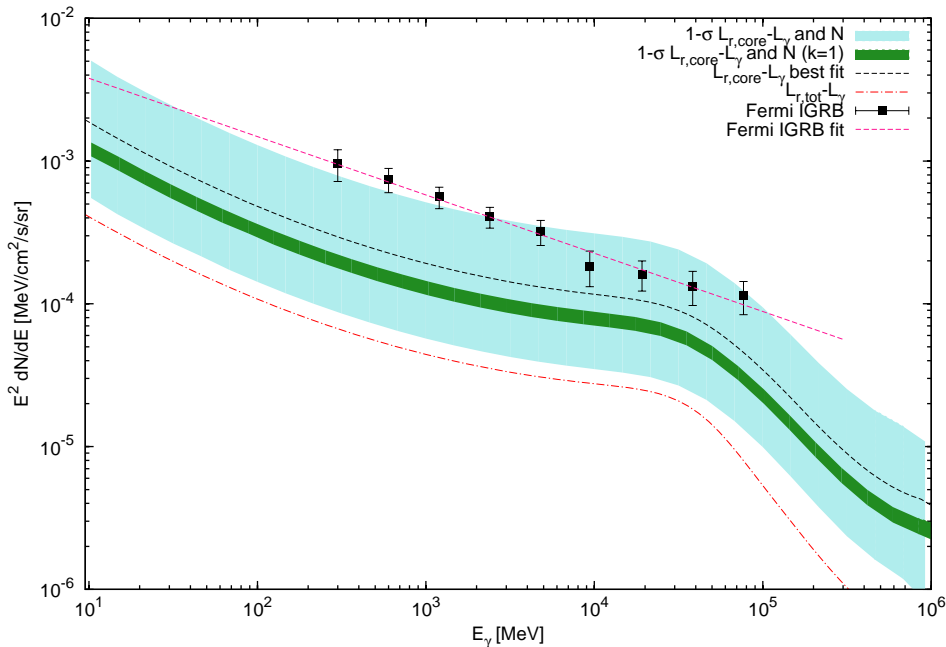


Figure 7. Diffuse γ -ray flux due to the MAGN as a function of γ -ray energy. The black squares correspond to the IGRB measured by *Fermi*-LAT (Abdo et al. 2010c) and best-fitted by the magenta dashed curve. The cyan shaded area derives from the 1σ uncertainty band on the $L_{r,\text{core}} - L_\gamma$ correlation and on the k parameter in the source count distribution. The dashed black line is obtained from the best fit on the $L_{r,\text{core}} - L_\gamma$ correlation. The green band corresponds to $k=1$ at 1σ C.L. (see discussion on Fig.5). The red dot-dashed curve shows the diffuse flux obtained when assuming a $L_{r,\text{tot}} - L_\gamma$ correlation.

ferent angular conversion factor in the RLF coefficients in Willott et al. (2001).

8. CONCLUSIONS

We have calculated the diffuse γ -ray emission from the population of MAGN at all redshifts.

We first established the existence (at 95% C.L.) of a correlation between the radio core ($L_{r,\text{core}}$) and the γ -ray (L_γ) luminosities of the MAGN detected by the *Fermi*-LAT. This correlation is substantially linear in the log plane, the radio luminosity being two orders of magnitude lower than the γ -ray luminosity. Extensive tests showed that this correlation is not likely to be a spurious effect due to the source distance. We also calculated the upper limits on the γ -ray emission from 33 radio-loud MAGN undetected by *Fermi*-LAT, and showed that these are compatible with the core radio – γ -ray luminosity correlation within 1σ errors.

We then used this correlation to infer a γ -ray luminosity function from a well established radio luminosity function, and further tested the former against the source count distribution measured by the *Fermi*-LAT. We correctly predicted the number of detected γ -ray sources, with values of the normalization factor k between the population of MAGN emitting in radio and γ rays that are close to one. Even when constraining $k = 1$, our γ -ray luminosity function matched the *Fermi*-LAT source count distribution, nicely confirming the robustness and simplicity of the luminosity correlation we derived. Using our γ -ray luminosity function, and after taking into account γ -ray absorption from a model of EBL, we predicted the diffuse γ -ray flux due to MAGN between 10 MeV and 1 TeV. We found an intensity of about $2 \cdot 10^{-4}$ MeV $\text{cm}^{-2}\text{s}^{-1}\text{sr}^{-1}$ at 1 GeV, embedded in a uncertainty band of nearly a factor of ten. At all *Fermi*-LAT energies, the best fit MAGN contribution is 20%-30% of the measured IGRB flux. The lower edge of the uncertainty band is about one order of magnitude smaller than the IGRB data while the

upper edge skims the data below a few GeV and slightly over-estimates them from a few GeV to around 50 GeV. At higher energies, the flux softens because of the EBL absorption. The intensity from MAGN integrated above 100 MeV is $9.83 \cdot 10^{-7}/2.61 \cdot 10^{-6}/8.56 \cdot 10^{-6}$ photons $\text{cm}^{-2} \text{s}^{-1} \text{sr}^{-1}$, when considering the lower/best fit/upper curve of the band reported in Fig. 7. These numbers represent 9.5%/25%/83% of the IGRB, respectively. The analogous calculation for the two blazar populations of BL Lacs and FSRQs gives $7.83^{+1.09}_{-2.34} \cdot 10^{-7}$ photons $\text{cm}^{-2} \text{s}^{-1} \text{sr}^{-1}$ (about 8% of the IGRB) for the former Abdo et al. (2010d) and $9.66^{+1.67}_{-1.09} 10^{-7}$ photons $\text{cm}^{-2} \text{s}^{-1} \text{sr}^{-1}$ (about 10% of the IGRB) for the latter Ajello et al. (2012). The integrated flux for star-forming galaxies Ackermann et al. (2012a) is instead $8.19^{+7.31}_{-3.89} \cdot 10^{-7}$ photons $\text{cm}^{-2} \text{s}^{-1} \text{sr}^{-1}$, which contributes 4.10% (14.8%) of the IGRB at minimum (maximum), and about 8% at its best fit value.

In conclusion, we have found that the cosmological population of faint and numerous MAGN gives a sizable diffuse extragalactic flux which, when added to the contribution from other sources (*i.e.* blazars, star-forming galaxies, millisecond pulsars (Faucher-Giguere & Loeb 2010; Siegal-Gaskins et al. 2011)), could entirely explain the observed IGRB. This scenario would leave very little room for more exotic sources, such as dark matter in the halo of our Galaxy (Calore et al. 2013).

M.D.M. and F.D. warmly acknowledge S. Massaglia for invaluable insights in the preliminary stage of this paper. M.A. acknowledges support from grant NNH09ZDA001N for the study of the origin of the Isotropic Gamma-ray Background. F.C. acknowledges support from the German Research Foundation (DFG) through grant BR 3954/1-1.

The *Fermi* LAT Collaboration acknowledges generous ongo-

ing support from a number of agencies and institutes that have supported both the development and the operation of the LAT as well as scientific data analysis. These include the National Aeronautics and Space Administration and the Department of Energy in the United States; the Commissariat à l’Energie Atomique and the Centre National de la Recherche Scientifique/Institut National de Physique Nucléaire et de Physique des Particules in France; the Agenzia Spaziale Italiana and the Istituto Nazionale di Fisica Nucleare in Italy; the Ministry of Education, Culture, Sports, Science and Technology (MEXT), High Energy Accelerator Research Organization (KEK), and Japan Aerospace Exploration Agency (JAXA) in Japan; and the K. A. Wallenberg Foundation, the Swedish Research Council, and the Swedish National Space Board in Sweden. Additional support for science analysis during the operations phase is gratefully acknowledged from the Istituto Nazionale di Astrofisica in Italy and the Centre National d’Etudes Spatiales in France.

REFERENCES

- Abazajian, K. N., Blanchet, S., & Harding, J. P. 2011, *Phys. Rev. D*, 84, 103007
- Abdo, A. A. et al. 2009a, *ApJ*, 700, 597
- Abdo, A. A. et al. 2009b, *ApJ*, 699, 31
- Abdo, A. A. et al. 2010a, *Science*, 328, 725
- Abdo, A. A. et al. 2010b, *ApJ*, 720, 912
- Abdo, A. A. et al. 2010c, *Phys. Rev. Lett.*, 104, 101101
- Abdo, A. A. et al. 2010d, *ApJ*, 720, 435
- Abdo, A. A. et al. 2010e, *ApJ*, 715, 429
- Ackermann, M. et al. 2011a, *ApJ*, 741, 30
- Ackermann, M. et al. 2011b, *ApJ*, 743, 171
- Ackermann, M. et al. 2012a, *Astrophys.J.*, 755, 164
- Ackermann, M. et al. 2012b, *Science*, 338, 1190
- Ajello, M., Shaw, M. S., Romani, R. W., et al. 2012, *ApJ*, 751, 108
- Akritas, M. G. & Siebert, J. 1996, *MNRAS*, 278, 919
- Barthel, P. D. 1989, *ApJ*, 336, 606
- Becker, R. H., White, R. L., & Edwards, A. L. 1991, *ApJS*, 75, 1
- Brown, A. M. & Adams, J. 2012, *MNRAS*, 421, 2303
- Burgess, A. M. & Hunstead, R. W. 2006, *ApJ*, 131, 114
- Burns, J. O., Feigelson, E. D., & Schreier, E. J. 1983, *ApJ*, 273, 128
- Calore, F., Di Mauro, M., & Donato, F. 2013, arXiv:astro-ph/1303.3284 To be submitted to *Phys. Rev. D*
- Dermer, C. D. & Schlickeiser, R. 1993, *ApJ*, 416, 458
- Dodson, R., Fomalont, E. B., Wiik, K., et al. 2008, *ApJS*, 175, 314
- Dondi, L. & Ghisellini, G. 1995, *MNRAS*, 273, 583
- Dunlop, J. S. & Peacock, J. A. 1990, *MNRAS*, 247, 19
- Ekers, R. D., Wall, J. V., Shaver, P. A., et al. 1989, *MNRAS*, 236, 737
- Evans, D. A., Hardcastle, M. J., Croston, J. H., Worrall, D. M., & Birkinshaw, M. 2005, *MNRAS*, 359, 363
- Fanaroff, B. L. & Riley, J. M. 1974, *MNRAS*, 167, 31P
- Faucher-Giguere, C.-A. & Loeb, A. 2010, *JCAP*, 1001, 005
- Finke, J. D., Razzaque, S., & Dermer, C. D. 2010, *ApJ*, 712, 238
- Geldzahler, B. J. & Fomalont, E. B. 1984, *AJ*, 89, 1650
- Ghirlanda, G., Ghisellini, G., Tavecchio, F., & Foschini, L. 2010, *MNRAS*, 407, 791
- Ghirlanda, G., Ghisellini, G., Tavecchio, F., Foschini, L., & Bonnoli, G. 2011, *MNRAS*, 413, 852
- Ghisellini, G., Tavecchio, F., & Chiaberge, M. 2005, *A&A*, 432, 401
- Gilmore, R. C., Madau, P., Primack, J. R., Somerville, R. S., & Haardt, F. 2009, *MNRAS*, 399, 1694
- Giovannini, G., Cotton, W. D., Feretti, L., Lara, L., & Venturi, T. 2001, *ApJ*, 552, 508
- Giovannini, G., Feretti, L., Gregorini, L., & Parma, P. 1988, *A&A*, 199, 73
- Grandi, P., Torresi, E., & on behalf of the FERMI-LAT collaboration. 2012a, ArXiv e-prints
- Grandi, P., Torresi, E., & Stanghellini, C. 2012b, *ApJ*, 751, L3
- Gregory, P. C. & Condon, J. J. 1991, *ApJS*, 75, 1011
- Henstock, D. R., Browne, I. W. A., Wilkinson, P. N., et al. 1995, *ApJS*, 100, 1
- Inoue, Y. 2011, *ApJ*, 733, 66
- Inoue, Y. & Totani, T. 2009, *ApJ*, 702, 523
- Israel, F. P., Raban, D., Booth, R. S., & Rantakyro, F. T. 2008, *A&A*, 483, 741
- Jones, P. A., Lloyd, B. D., & McAdam, W. B. 2001, *MNRAS*, 325, 817
- Kadler, M., Eisenacher, D., Ros, E., et al. 2012, *A&A*, 538, L1
- Kataoka, J. et al. 2011, *ApJ*, 740, 29
- Katsuta, J., Tanaka, Y. T., Stawarz, L., et al. 2013, *A&A*, 550, A66
- Kazanas, D. & Perlman, E. 1997, *ApJ*, 476, 7
- Kuehr, H., Witzel, A., Pauliny-Toth, I. I. K., & Nauber, U. 1981, *A&AS*, 45, 367
- Laing, R. A., Riley, J. M., & Longair, M. S. 1983, *MNRAS*, 204, 151
- Lara, L., Giovannini, G., Cotton, W. D., et al. 2004, *A&A*, 421, 899
- Linfield, R. & Perley, R. 1984, *ApJ*, 279, 60
- Mantovani, F., Mack, K.-H., Montenegro-Montes, F. M., Rossetti, A., & Kraus, A. 2009, *A&A*, 502, 61
- Maraschi, L., Ghisellini, G., & Celotti, A. 1992, *ApJ*, 397, L5
- Massardi, M., Ekers, R. D., Murphy, T., et al. 2008, *MNRAS*, 384, 775
- Massaro, F. & Ajello, M. 2011, *ApJ*, 729, L12
- Mazin, D. & Raue, M. 2007, *A&A*, 471, 439
- Morganti, R., Killeen, N. E. B., & Tadhunter, C. N. 1993, *MNRAS*, 263, 1023
- Mullin, L. M., Hardcastle, M. J., & Riley, J. M. 2006, *MNRAS*, 372, 113
- Nagar, N. M., Wilson, A. S., & Falcke, H. 2001, *ApJ*, 559, L87
- Narumoto, T. & Totani, T. 2006, *ApJ*, 643, 81
- Neff, S. G., Roberts, L., & Hutchings, J. B. 1995, *ApJS*, 99, 349
- Nolan, P. L. et al. 2012a, *ApJS*, 199, 31
- Nolan, P. L. et al. 2012b, *VizieR Online Data Catalog*, 219, 90031
- Padovani, P., Ghisellini, G., Fabian, A. C., & Celotti, A. 1993, *MNRAS*, 260, L21
- Pauliny-Toth, I. I. K., Kellermann, K. I., Davis, M. M., Fomalont, E. B., & Shaffer, D. B. 1972, *AJ*, 77, 265
- Pearson, T. J., Blundell, K. M., Riley, J. M., & Warner, P. J. 1992, *MNRAS*, 259, 13P
- Perley, R. A., Roser, H.-J., & Meisenheimer, K. 1997, *A&A*, 328, 12
- Razzaque, S., Dermer, C. D., & Finke, J. D. 2009, *ApJ*, 697, 483
- Salamon, M. H. & Stecker, F. W. 1994, *ApJ*, 430, L21
- Salamon, M. H. & Stecker, F. W. 1998, *ApJ*, 493, 547
- Siegal-Gaskins, J. M., Reesman, R., Pavlidou, V., Profumo, S., & Walker, T. P. 2011, *Mon.Not.Roy.Astron.Soc.*, 415, 1074S
- Spinrad, H., Marr, J., Aguilar, L., & Djorgovski, S. 1985, *PASP*, 97, 932
- Stawarz, L., Kneiske, T. M., & Kataoka, J. 2006, *ApJ*, 637, 693
- Stecker, F. W., Malkan, M. A., & Scully, S. T. 2006, *ApJ*, 648, 774
- Stecker, F. W. & Salamon, M. H. 1996, *ApJ*, 464, 600
- Stecker, F. W., Salamon, M. H., & Malkan, M. A. 1993, *ApJ*, 410, L71
- Stecker, F. W. & Venters, T. M. 2011, *ApJ*, 736, 40
- Tingay, S. J., Reynolds, J. E., Tzioumis, A. K., et al. 2002, *ApJS*, 141, 311
- Urry, C. M. & Padovani, P. 1995, *PASP*, 107, 803
- Venters, T. M. 2010, *ApJ*, 710, 1530
- Venters, T. M., Pavlidou, V., & Reyes, L. C. 2009, *ApJ*, 703, 1939
- Venturi, T., Dallacasa, D., & Stefanachi, F. 2004, *A&A*, 422, 515
- Wilkinson, P. N., Akujor, C. E., Cornwell, T. J., & Saikia, D. J. 1991, *MNRAS*, 248, 86
- Willott, C. J., Rawlings, S., Blundell, K. M., Lacy, M., & Eales, S. A. 2001, *MNRAS*, 322, 536
- Wright, A. E., Griffith, M. R., Burke, B. F., & Ekers, R. D. 1994, *ApJS*, 91, 111
- Yan, D., Zeng, H., & Zhang, L. 2012, *MNRAS*, 422, 1779
- Yuan, Z. & Wang, J. 2012, *ApJ*, 744, 84